Assembly of a Mixture of Isomeric BChl *c* from *Chlorobium limicola* As Determined by Intermolecular $^{13}C-^{13}C$ Dipolar Correlations: Coexistence of Dimer-Based and Pseudo-Monomer-Based Stackings†

Yoshinori Kakitani,‡ Hiroyoshi Nagae,§ Tadashi Mizoguchi,‡,|| Ayako Egawa,⊥ Kengo Akiba,⊥ Toshimichi Fujiwara,⊥ Hideo Akutsu,⊥ and Yasushi Koyama*,‡

Faculty of Science and Technology, Kwansei Gakuin University, Gakuen, Sanda 669-1337, Japan, Kobe City University of Foreign Studies, Gakuen-Higashimachi, Nishi-ku, Kobe 651-2187, Japan, Department of Bioscience and Biotechnology, Ritsumeikan University, Nojihigashi, Kusatsu 525-8577, Japan, and Institute for Protein Research, Osaka University, Yamadaoka, Suita 565-0871, Japan

Received December 19, 2005; Revised Manuscript Received April 10, 2006

ABSTRACT: A mixture of bacteriochlorophyll (BChl) *c* isomers was extracted from the cells of *Chlorobium limicola* that were grown in the media of ^{13}C-enriched and natural-abundance isotopic compositions. The magic-angle spinning ^{13}C NMR proton-driven spin-diffusion spectra were recorded with mixing times of 50, 100, and 250 ms for two different kinds of in vitro aggregates, one consisting of pure [^{13}C]BChl *c* and the other consisting of a 1:1 mixture of [^{13}C]BChl *c* and [^{12}C]BChl *c*; those peaks whose intensities were reduced to $\sim 1/4$ by this dilution were assigned to intermolecular $^{13}C-^{13}C$ dipolar correlation peaks. On the other hand, the nearest-neighbor intermolecular carbon−carbon close contacts with distances of 4−6 Å were simulated, to predict observed correlation peaks, for six different models of BChl *c* assembly. They include weakly overlapped monomers forming structure **1** and structure **2**, strongly overlapped dimers forming straight and inclined columns, and weakly overlapped dimers forming aligned and displaced layers. Comparison between the observed correlation peaks and the predicted carbon−carbon close contacts, for both the macrocycles and the side chains, led us to a conclusion that the weakly overlapped dimers forming displaced layers are most likely the assembly of the BChl *c* molecules in the aggregate.

Green photosynthetic bacteria contain a kind of antenna complexes called "chlorosomes" consisting of lipid membrane and rod elements, which are cylindrical aggregates of bacteriochlorophyll (BChl)[1] *c* molecules (see refs *1*−*3* for reviews). (Hereafter, we call this assembly a chlorosome, instead of "the rod element", according to ordinary convention.) Chlorosomes consist of a mixture of BChl *c* isomers having two different stereoisomeric configurations of the hydroxyethyl group, i.e., *R* and *S*, and three different side chains attached to the C8 position, i.e., ethyl, propyl, and isobutyl abbreviated as E, P, and I, respectively. In *Chlorobium limicola*, for example, the isomeric composition includes an ≈4:5:1 (3^1R)-8-ethyl-12-ethyl bacteriochlorophyll c_F (*R*[E,E]):(3^1R)-8-propyl-12-ethyl bacteriochlorophyll c_F (*R*[P,E]):(3^1S)-8-isobutyl-12-ethyl bacteriochlorophyll c_F (*S*[I,E]) ratio, whereas in *Chlorobium tepidum*, there is an ≈7:2:1 *R*[E,E]:*R*[P,E]:(3^1S)-8-propyl-12-ethyl bacteriochlorophyll c_F (*S*[P,E]) + *S*[I,E] ratio (see Scheme 1 for their structures). Thus, the *R*-isomers having small and medium side chains make up the major component, and the *S*-isomers having large and medium side chains make up the minor component in both chlorosomes. The structures of in vitro aggregates are useful as a basis of elucidating the structure of real chlorosomes. For the structural determination, X-ray crystallography has not been successfully used, because it is difficult to form a three-dimensional crystal of such a mixture of stereoisomers having a long farnesyl side chain.

High-resolution NMR spectroscopy in solution (*4*−*6*) and solid-state magic-angle spinning (MAS) NMR spectroscopy (*7*−*9*), electronic-absorption spectroscopy (*10*, *11*), and molecular modeling (*12*) have been extensively applied to elucidate the structures of in vitro aggregates and chlorosomes, and two different forms of aggregate have been proposed (see ref *1* for a review): one consisting of a monomer-based stacking called "the parallel-chain model" (*5*, *6*, *8*−*12*) and the other consisting of a dimer-based stacking called "the antiparallel-chain model" (*4*, *7*). Even a basic question concerning the assembly of macrocycles, i.e., monomer-based stacking or dimer-based stacking, remains to be answered.

† This work has been supported by an Open Research Center Project grant from the Ministry of Education, Culture, Sports, Science and Technology, Japan, and an International Joint Research Grant from New Energy and Industrial Technology Development Organization (NEDO), Japan (to Y. Koyama). Y. Kakitani has been supported by Research Fellowships of the Japan Society for the Promotion of Science for Young Scientists.

* To whom correspondence should be addressed. Telephone and fax: +81-79-565-8408. E-mail: ykoyama@kwansei.ac.jp.

‡ Kwansei Gakuin University.

§ Kobe City University of Foreign Studies.

|| Ritsumeikan University.

⊥ Osaka University.

[1] Abbreviations: BChl, bacteriochlorophyll; CP, cross polarization; MAS, magic-angle spinning; NOE, nuclear Overhauser effect; PDSD, proton-driven spin diffusion; *R*[E,E], (3^1R)-8-ethyl-12-ethyl bacteriochlorophyll c_F; RFDR, radio frequency-driven dipolar recoupling; *R*[P,E], (3^1R)-8-propyl-12-ethyl bacteriochlorophyll c_F; *S*[I,E], (3^1S)-8-isobutyl-12-ethyl bacteriochlorophyll c_F; SPC-5, supercycled POST-C5; *S*[P,E], (3^1S)-8-propyl-12-ethyl bacteriochlorophyll c_F.

10.1021/bi0525728 CCC: $33.50
Published on Web 05/26/2006

Scheme 1

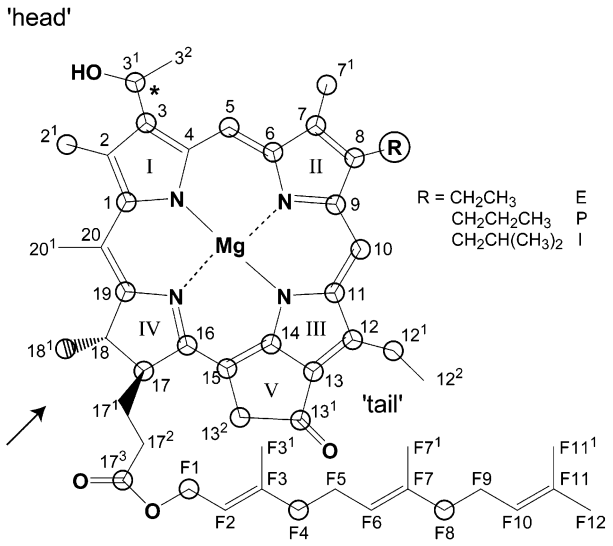

High-resolution NMR spectroscopy, using the ring-current effects on the ^{1}H and ^{13}C chemical shifts (often called "aggregation shifts") due to the macrocycles of neighboring BChl *c* molecules or the $^{1}H-^{1}H$ intermolecular nuclear Overhauser effect (NOE) correlations between the peripheral parts of neighboring BChl *c* molecules, has been used to elucidate the structural motifs of smaller aggregates in suspension. It turned out that purified isomers give rise to different forms of the aggregate, depending on the *R*- and *S*-stereoisomeric configurations and on the bulkiness of the C8 side chain. (1) The *R*[E,E] aggregate exhibiting Q_y absorption at 675 nm forms the piggyback dimer (*13*−*16*). (2) The *S*[I,E] aggregate exhibiting Q_y absorption at 745 nm forms a monomer-based stacking (*17*) in two different forms, i.e., structure **1** and structure **2** (*18*). (3) The *R*[E,E] aggregate absorbing at 705 nm uses the dimer-based stacking to form a straight column (*19*). (4) The *R*[P,E] aggregate absorbing at 720 and 745 nm uses a dimer-based stacking to form an inclined column (*6*). Most importantly, there are two different types of aggregates exhibiting Q_y absorption at ∼745 nm, as chlorosomes do: one consisting of the monomer-based stacking and the other consisting of the dimer-based stacking. Both form a stairlike arrangement of the macrocycles. The simulation of the red shift of the Q_y absorption and the calculation of steric energy for a set of aggregates of BChl *c* isomers (*6*) proved that both types of stacking can form larger aggregates exhibiting Q_y absorption at ∼745 nm, which were named "B745m" and "B745d" (m and d refer to the monomer-based and dimer-based stackings, respectively; see Figure 6 of ref *6*).

As an extension of such studies on small in vitro aggregates in suspension as models for chlorosomes, the structural determination of a large aggregate of BChl *c* by MAS NMR spectroscopy is a key technique in the structural determination of solid-state aggregates and chlorosomes. Most recently, Umetsu et al. (*20*) examined the structure of a solid-state *R*[E,E] aggregate absorbing at 740 nm by MAS ^{13}C NMR spectroscopy using the radio frequency-driven dipolar recoupling (RFDR) and the proton-driven spin-diffusion (PDSD) correlation techniques. Doubling of carbon signals led them to conclude that two forms of aggregates exhibiting type A and type B signals coexist, which were assigned, on the basis of the aggregation shifts, to dimer-based stacking and monomer-based stacking, respectively. The authors concluded that two different types of solid-state species were present in the same aggregate.

On the other hand, the determination of the structure of the in vitro aggregate of the BChl *c* extract is important because of its relevance to that of chlorosomes. The MAS RFDR ^{13}C dipolar correlation spectrum of an in vitro aggregate of the BChl *c* extract from *Chl. tepidum* was found to be indistinguishable from that of chlorosomes, indicating that their structures are very similar as far as the particular spectroscopic method is concerned (*7*−*9*).

In this investigation, we recorded the PDSD spectra (hereafter abbreviated as "the spin-diffusion spectra" as well) of an in vitro aggregate of a mixture of BChl *c* isomers extracted from the cells of *Chl. limicola* (hereafter abbreviated as "the solid-state aggregate of BChl *c*"). We ascribed those peaks, whose intensity decreased to $\sim^{1}/_{4}$ after the 50% dilution of [^{13}C]BChl *c* with [^{12}C]BChl *c*, to intermolecular $^{13}C-^{13}C$ dipolar coupling. Then, we simulated the intermolecular carbon−carbon contacts with distances in the 4−6 Å region to predict the intermolecular correlation peaks for a set of models that were based on the above-mentioned, high-resolution NMR and electronic-absorption spectroscopies of smaller aggregates in suspension.

We have addressed these two specific questions. (1) How are the BChl *c* molecules assembled in the aggregate of an isomeric mixture from *Chl. limicola* in the solid state? We tried to answer the long-standing question of whether there is monomer-based stacking or dimer-based stacking. (2) How does the assembly of BChl *c* in a large aggregate in the solid state compare to, or contrast to, those in the smaller aggregates in suspension? How are those structures stabilized by various kinds of intermolecular interactions?

The results lead us to a conclusion that the structure of the solid-state aggregate of BChl *c* contains both types of stackings, i.e., the dimer-based stacking and the (pseudo) monomer-based stacking. The structure of the large solid-state aggregate of BChl *c* is found to reflect additional intermolecular interactions other than those in the smaller aggregates in suspension.

MATERIALS AND METHODS

Culturing ^{13}C-Enriched Cells. The cells of *Chl. limicola* f. sp. *thiosulfatophilum*, with a natural-abundance isotopic composition, were grown anaerobically at 27 °C in dim light in the medium of Wahlund et al. (*21*), to which casamino acids (1.0 g/L) and vitamin B_1 hydrochloride (50 mg/L) were added. The ^{13}C-enriched cells were grown by replacing the carbon source, $NaH^{12}CO_3$, with $NaH^{13}CO_3$ (99.9%, MassTrace Inc.); the relative amount of the latter was increased gradually (for the cells to be adapted to ^{13}C) in the following order: 1.5 g/L for the first and second culturing and 1.75 g/L (the total amount) for the last culturing. Neither casamino acids nor vitamin B_1 hydrochloride (containing ^{12}C) was added in this particular medium.

Preparation of BChl c Aggregates. A mixture of BChl *c* isomers was extracted from the cells as described previously (*22*). The degradation products that were generated during the extraction procedure were removed by HPLC using the following conditions: a column with an internal diameter

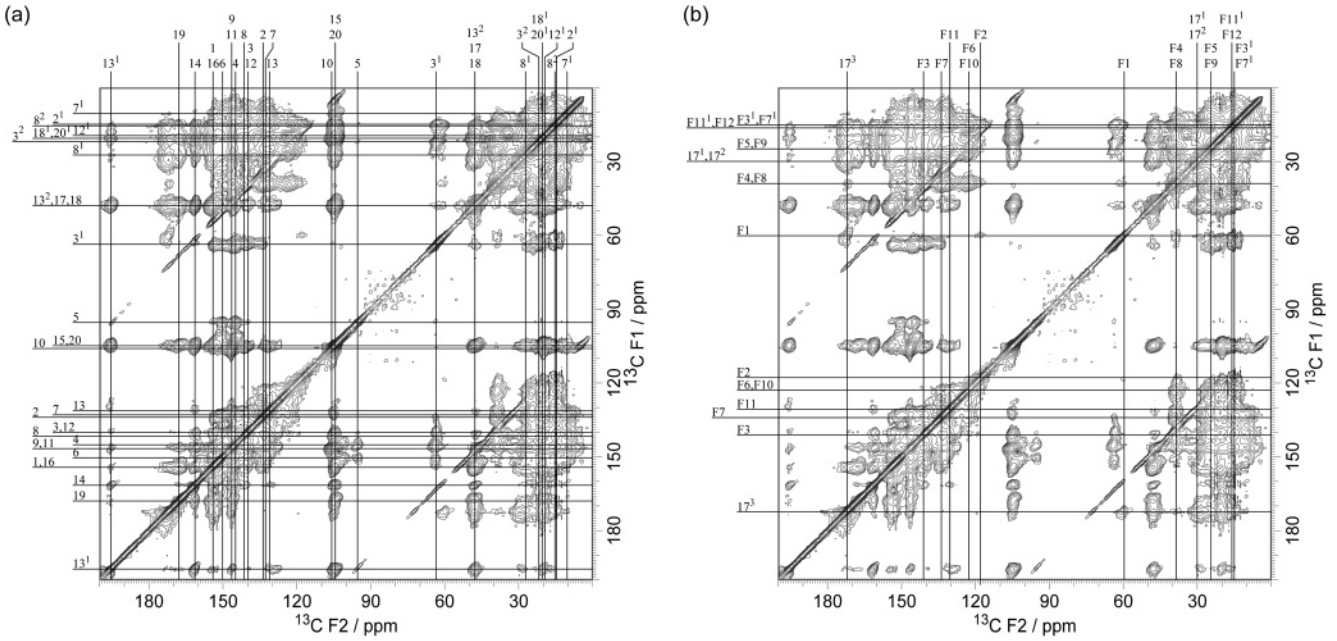

FIGURE 1: Spin-diffusion spectrum (mixing time of 100 ms) of the solid-state aggregate of 100% [^{13}C]BChl *c*. The chemical shift values for the ^{13}C signals with regard to (a) the macrocycle and (b) the side chain are shown, as a guide for eyes, to identify the ^{13}C−^{13}C dipolar correlation peaks (see Scheme 1 for the typification of the carbon atoms).

of 20 mm and a length of 250 mm, packed with 5 μm VX-ODS (Shinwa Chemical Industries, Ltd.), an eluent of methanol, a flow rate of 3.5 mL/min, and a detection wavelength of 435 nm. The components eluting before the BChl *c* isomeric mixture were discarded. The ^{13}C enrichment factor was determined by ^{1}H NMR spectroscopy using the area under the ^{1}H−^{13}C coupled peaks to be ∼100% for the macrocycle and 76% for the farnesyl group.

For NMR measurements, two different kinds of aggregates of the above isomeric mixture in the solid state, i.e., one consisting of ^{13}C-enriched BChl *c* only ("100% [^{13}C]BChl *c*") and the other consisting of a 1:1 mixture of ^{13}C-enriched BChl *c* and BChl *c* with a natural-abundance isotopic composition ("50% [^{13}C]BChl *c*"), were prepared as follows. BChl *c* in an acetone solution of each composition was dried in vacuo and dissolved in a minimum amount of dichloromethane, and 9 equiv of *n*-hexane was added; the aggregate that precipitated at ∼0 °C was spun down (24000*g* for 30 min), dried in vacuo, and powdered with an agate mortar.

NMR Measurements. Each sample was transferred to a sample rotor with an internal diameter of 4 mm. NMR spectra were recorded by using a Varian Infinity-plus 500 spectrometer (magnetic field of 11.7 T, resonance frequencies of 125.66 MHz for ^{13}C and 499.698 MHz for ^{1}H under MAS). The RFDR spectra (*23*, *24*) were recorded under the conditions of cross polarization (CP): contact time of 2.2 ms, RFDR mixing time of 1.28 ms, MAS rate of 12.5 kHz, data accumulation for 23 h, and temperature of 10 °C, whereas the supercycled POST-C5 (SPC-5) spectra (*25*) were recorded under the conditions of CP: contact time of 2.2 ms, SPC-5 mixing time of 1.1 ms, MAS rate of 11.0 kHz, data accumulation for 24 h, and temperature of −30 °C. The PDSD spectra ("the spin-diffusion spectra") (*26*−*28*) were recorded with CP: contact time of 2.2 ms, mixing times of 57.6, 115.2, and 244.8 ms (hereafter approximated as 50, 100, and 250 ms, respectively), MAS rate of 12.5 kHz, data accumulation for 23 h, and temperature of 10 °C. The ^{13}C chemical shifts were referenced to the methyl peak of hexamethylbenzene resonating at 16.47 ppm from tetramethylsilane.

Model Building. Models of the three-dimensional aggregate of BChl *c* were built by arranging a repeating subunit (a monomer or a piggyback dimer) on the lattice points defined by three fundamental translational vectors, **a**, **b**, and **c**. We calculated the distances of all pairs of carbon atoms in the same BChl *c* molecule as well as those between a pair of BChl *c* molecules based on the relevant models. In building each model, the distance between a pair of macrocycles was assumed to be 4.5 Å and the distance between the oxygen atom in the hydroxyethyl group and the Mg atom in the macrocycle to be 2.7 Å. In the rest of the model, van der Waals radii, i.e., 1.70 Å for C, 1.55 Å for N, and 1.40 Å for O, were assumed. To obtain the best agreement between the observed ^{13}C−^{13}C correlation peaks and the simulated carbon−carbon close contacts, the mutual arrangement of the columns was adjusted in each model.

RESULTS

Extraction of Intermolecular ^{13}C−^{13}C Dipolar Correlation Peaks for the Structural Determination. Figure 1 shows the spin-diffusion spectrum of the solid-state aggregate of BChl *c*. The chemical shift values for the signals of ^{13}C for (a) the macrocycle and (b) the side chain (defined as the region between C17^{1} and CF12; see Scheme 1 for the identification of carbon atoms) are shown as a guide for eyes to identify the ^{13}C−^{13}C dipolar correlation peaks. The ^{13}C signals for the macrocycle were assigned by using an RFDR spectrum starting from the isolated signal of C13^{1} in the keto carbonyl group and that of C3^{1} in the hydroxyethyl group; the two sets of assignments were in complete agreement. Some signals due to the macrocycle and all the signals due to the farnesyl group were assigned by the use of an SPC-5 spectrum; this technique identifies the nearest-neighbor and the second-nearest-neighbor ^{13}C−^{13}C correlation peaks.

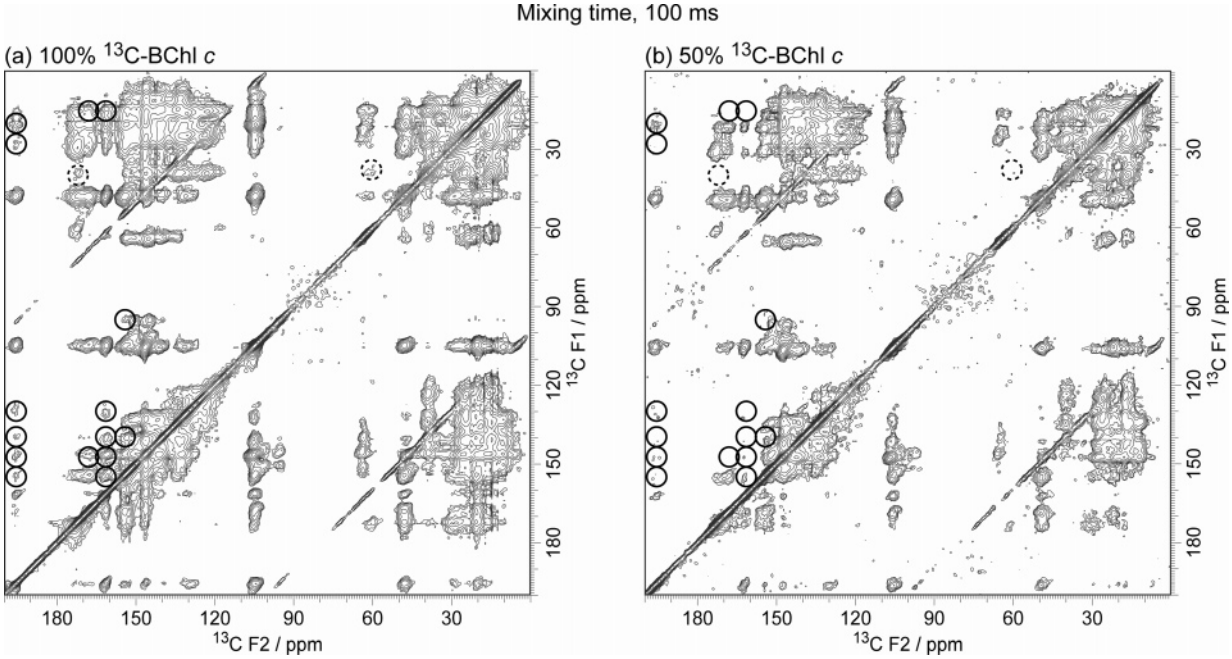

FIGURE 2: Intermolecular $^{13}C-^{13}C$ correlation peaks, identified in the spin-diffusion spectrum (mixing time of 100 ms) for the carbon atoms in the macrocycle (solid circles) and those in the side chain (dashed circles). The intensities of those peaks decrease to $\sim^1/_4$ upon dilution of [^{13}C]BChl *c* from (a) 100 to (b) 50%.

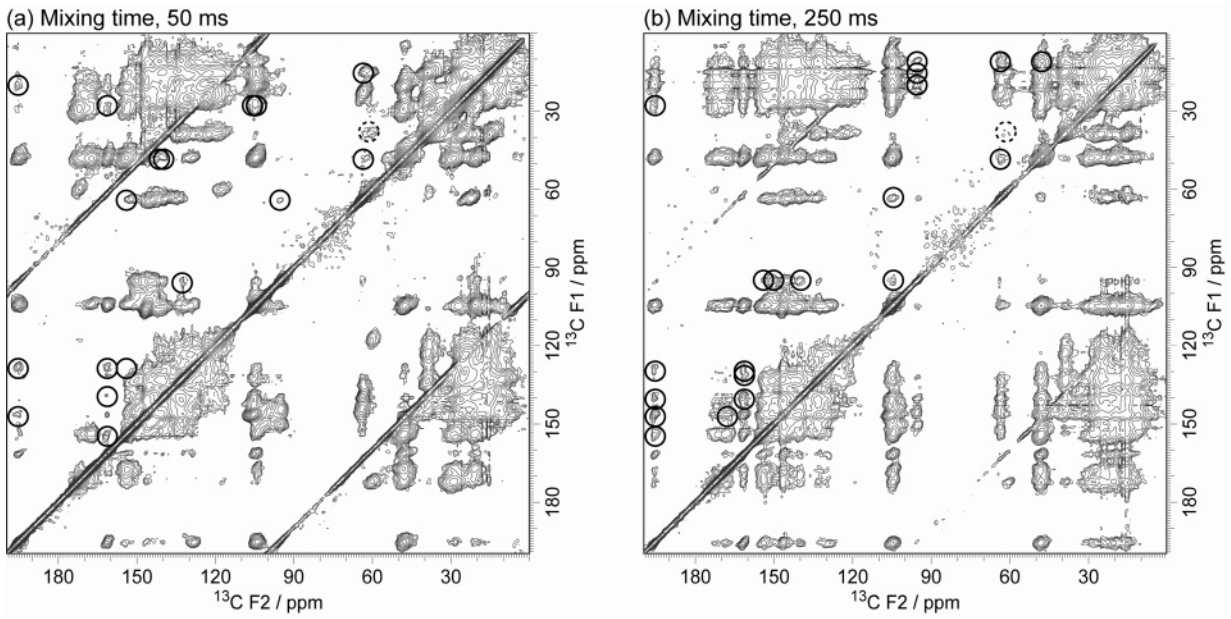

FIGURE 3: Intermolecular $^{13}C-^{13}C$ correlation peaks in the spin-diffusion spectra of 100% [^{13}C]BChl *c* [mixing times of (a) 50 and (b) 250 ms]. Assignments are given for the carbon atoms in the macrocycle (solid circles) and the side chain (dashed circles). See Figure 1 for their chemical shift values.

Figure 2 shows the spin-diffusion spectra of two different types of BChl *c* aggregates: (a) 100% [^{13}C]BChl *c* and (b) 50% [^{13}C]BChl *c*. The spectra were recorded with a mixing time of 100 ms. On dilution of [^{13}C]BChl *c* from 100 to 50%, the intramolecular correlation peaks decreased in intensity by 50% (a decrease in the [^{13}C]BChl *c* concentration), whereas the intermolecular correlation peaks decreased in intensity by 25% (the chance of forming the [^{13}C]BChl−[^{13}C]BChl pair out of four different pairs). The intermolecular correlation peaks are represented by solid circles in the figure. Figure 3 shows the spin-diffusion spectra recorded with mixing times of (a) 50 and (b) 250 ms; the intermolecular correlation peaks were assigned in a similar way. All those intermolecular correlation peaks thus extracted are listed in Table 1, and the relevant carbon atoms are represented by circles in Scheme 1. They are almost homogeneously located around the macrocycle, a fact which supports our strategy of determining the assembly of macrocycles by the use of those intermolecular $^{13}C-^{13}C$ dipolar correlations that have been clearly identified in the spin-diffusion spectra. However, the correlation peaks to be used in the structural analysis are limited in number, because of the strong overlap of the intramolecular and intermolecular correlation peaks as seen in Figures 1−3.

Possible Models for the Assembly of Macrocycles Based on the Previous Results of Smaller Aggregates in Solution.

Table 1: Intermolecular $^{13}C-^{13}C$ Dipolar Correlation Peaks Identified in the Proton-Driven Spin-Diffusion Spectra Recorded with Different Mixing Times

50 ms		100 ms		250 ms	
$1/3^1$	$13/13^1$	1/3	13/14	1/5	7/14
$2^1/3^1$	13/14	1/5	$13^1/16$	$2^1/5$	$7^1/13^2$
$3/13^2$	13/16	$2^1/14$	14/16	3/5	$8^1/13^1$
$3^1/5$	$13^1/18^1$	$2^1/19$	F1/(F4/F8)	$3/13^1$	$(9/11)/13^1$
$3^1/13^2$	14/16	$3/13^1$		3/14	(9/11)/19
5/7	17^3/(F4/F8)	3/14		$3^1/7^1$	$12/13^1$
$8/13^2$	F1/(F4/F8)	$8^1/13^1$		$3^1/15$	12/14
$8^1/10$		$(9/11)/13^1$		$3^1/17$	$13/13^1$
$8^1/14$		(9/11)/14		5/6	13/14
$8^1/15$		(9/11)/19		$5/7^1$	$13^1/16$
$(9/11)/13^1$		$12^1/13^1$		$5/12^1$	F1/(F4/F8)
12/14		$13/13^1$		5/15	

Since the stacking of macrocycles is based on the coordination bonds between the oxygen atom in the hydroxyethyl group and the Mg atom in the center of the macrocycle (Scheme 1), a column consisting of either monomer-based or dimer-based stacking can be formed along the axis connecting ring I and ring III. With respect to the long axis of the column, the side chains extend along one side in monomer-based stacking, whereas they extend along both sides in dimer-based stacking. Therefore, in both cases, the side chains in various conformations prevent further association of the stacked columns to form a three-dimensional regular structure in smaller aggregates. Here, the assembly of the macrocycles is two-dimensional in nature.

Figure 4 schematically presents possible models for the two-dimensional assemblies of the macrocycles we are going to examine. In the figure, each part of the BChl *c* molecule is shown by symbols, including a rectangle (the macrocycle), a bent arrow (the hydroxyl group coordinating the central Mg atom), ═O (the keto carbonyl group), and a triangle (the root of the side chain). When the BChl *c* molecule is viewed from the direction of the side chain (see the arrow in Scheme 1), both the macrocycle and the side chain are shown with empty open symbols, whereas when BChl *c* is viewed from the opposite direction, they are shown by shadowed and painted symbols. These models are two-dimensional extensions of *the structural motifs* that have been determined either by high-resolution NMR spectroscopy using the ^1H and ^{13}C aggregation shifts and the $^1H-^1H$ NOE correlations or by electronic-absorption spectroscopy using the red shift of the Q_y absorption (see the introductory section).

There have been five different structural motifs identified, and they can be classified into two monomer-based stackings and three dimer-based stackings (see Figure 4). In the monomer-based stacking named "weakly overlapped monomers", two different structures, (a) structure **1** and (b) structure **2**, have been identified by the above-mentioned NMR techniques (*18*). In the dimer-based stacking called "strongly overlapped dimers", the ^1H and ^{13}C aggregation shifts showed that both (c) the "straight" and (d) the "inclined" columns can be formed, although the $^1H-^1H$ NOE correlations detected only the straight column (*19*). The measurement and simulation of the shift of the Q_y absorption identified both the straight and inclined columns (*6*). In the dimer-based stacking called (e) "weakly overlapped dimers", only an assembly forming "aligned" layers was identified by NMR spectroscopy using the ^1H and ^{13}C aggregation shifts (*6*). (f) The last model named "weakly overlapped dimers forming displaced layers" (macrocycles are aligned in the alternate directions to form a single layer) has never

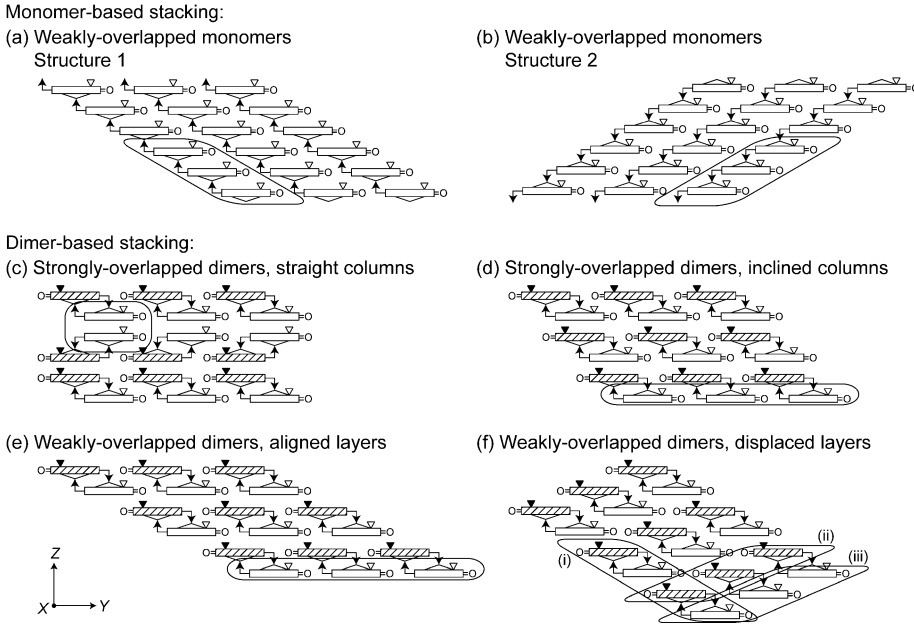

FIGURE 4: Schematic presentation of the models that were used in the determination of the two-dimensional assemblies of the BChl *c* molecules. Each part of the BChl molecules is shown by using different symbols: rectangle (the macrocycle), bent arrow (the hydroxyethyl group coordinating the central Mg atom), ═O (the keto carbonyl group), and triangle (the root of the side chain). When viewed from the direction indicated by an arrow in Scheme 1, both the macrocycle and the side chain are shown with empty symbols, whereas when viewed from the opposite direction, they are shown by shaded and painted symbols, respectively. The models are classified into two monomer-based stackings and four dimer-based stackings. Monomer-based stackings named weakly overlapped monomers form (a) structure **1** and (b) structure **2**. Dimer-based stackings called strongly overlapped dimers form (c) straight and (d) inclined columns, while those called weakly overlapped dimers form (e) aligned and (f) displaced layers. Models a−e are based on the results of high-resolution NMR and electronic-absorption spectroscopies of smaller aggregates in suspension (see the text for the details). The last form of assembly (f) has been identified, for the first time, in the solid-state aggregate of BChl *c* presented here.

been identified by high-resolution NMR spectroscopy in small aggregates in suspension. This may be simply because the intercolumn contacts could not be easily detected by using the $^{1}H-^{1}H$ NOE correlations in the above-mentioned small aggregates in suspension; the ^{1}H and ^{13}C aggregation shifts would not differentiate either the aligned layers or the displaced layers. This type of assembly of macrocycles emerged during our analysis of the in vitro aggregate of the BChl *c* isomeric mixture in the solid state, the details of which are described below.

Most importantly, the stairlike arrangement of the macrocycles is commonly seen in both the weakly overlapped monomers (structure **1** and structure **2**) and the weakly overlapped dimers (aligned and displaced layers). All those assemblies in the aggregates actually give rise to similar shifts of the ^{1}H and ^{13}C signals due to the ring-current effect, and also the shifts of the Q_y absorption to 745 nm due to the transition dipole−transition dipole interaction. Therefore, only the $^{13}C-^{13}C$ dipolar correlations, reflecting local intermolecular interactions, can differentiate those structures.

Assembly of Macrocycles Determined by Comparison between the Observed Intermolecular $^{13}C-^{13}C$ Dipolar Correlations and the Simulated Intermolecular Carbon−Carbon Short Contacts in Different Models. Figure 5 shows, in color, the observed intermolecular correlation peaks. They are classified in terms of the mixing times: 50 (yellow), 100 (blue), and 250 ms (red). Those correlation peaks that were identified at both 50 and 100 ms (green) and at both 100 and 250 ms (magenta) are also classified. The figure also shows, in black, the simulation of intermolecular contacts between a pair of carbon atoms based on the models shown in Figure 4; they are classified in terms of carbon−carbon distances, i.e., <4 (filled circles), 4−5 (empty double circles), and 5−6 Å (empty circles). When the assignment of the intermolecular $^{13}C-^{13}C$ dipolar correlation peaks was not clear due to the overlap of a pair of peaks, one of the possible assignments was chosen depending on the carbon−carbon contacts that were predicted.

Table 2 summarizes the results of comparison; each score is defined as the number of correctly predicted correlation peaks divided by the number of total observed correlation peaks. Agreement and disagreement, in each model, between the observed $^{13}C-^{13}C$ correlation peaks and the predicted carbon−carbon short contacts can be characterized as follows (see both Figure 5 and Table 2). Neither (a) structure **1** nor (b) structure **2** of weakly overlapped monomers explains the observed correlation peaks in the two diagonal regions, because no intermolecular short contacts are predicted at all. These models explain short contacts in the off-diagonal regions only partially. The scores of agreement for the average of three mixing times are as low as 36 and 34% in structure **1** and structure **2**, respectively. (c) Strongly overlapped dimers forming a straight column explain the observed intermolecular correlation peaks fully in the diagonal region, but only partly in the off-diagonal region; some observed intermolecular correlation peaks in the off-diagonal region are left unexplained. The averaged score is as high as 75%. This is partly due to the complete overlap of a pair of macrocycles (see Figure 4c), which predicts a large number of correlation peaks in the diagonal region. (d) Strongly overlapped dimers forming an inclined column explain the observed intermolecular correlation peaks in both the diagonal and off-diagonal regions except for those in the central region. Therefore, agreement between the observed and predicted correlation peaks is fairly good; the averaged score of agreement is 66%. (e) Weakly overlapped dimers forming aligned layers explain the observed intermolecular correlation peaks better in the diagonal region than in the off-diagonal region, although many observed correlation peaks are left unexplained in both regions. The averaged score is 52%. (f) Weakly overlapped dimers forming displaced layers explain the observed intermolecular correlation peaks very nicely. The averaged score of agreement is the highest of any, i.e., 81%. Interestingly, the score tends to increase in the order of mixing time in this particular model: 65% (50 ms) < 87% (100 ms) < 91% (250 ms). In other words, this assembly of the BChl *c* molecules gives rise to the extremely high score of 91% with regard to the ^{13}C dipolar correlation peaks detected at the longest mixing time. This systematic increase in the score with the increasing mixing time can be explained in terms of the spin-diffusion processes reflecting this particular structure, the details of which are presented as Supporting Information (spin-diffusion processes reflecting the structure of the BChl *c* aggregate in the solid state).

Thus, among the models examined here, the model of weakly overlapped dimers forming displaced layers gives rise to the best agreement.

(As shown in Figure 4f, no direct hydrogen bonding between the hydroxyethyl OH group and the keto C═O group occurs in this particular assembly of macrocycles. A pair of water molecules may form hydrogen bonds with those groups.)

Interaction between the Side Chains and the Structure of the BChl c Aggregate. We have tried to identify the intermolecular $^{13}C-^{13}C$ correlation peaks in the spin-diffusion spectra due to the side chains (Figure 1b). Since the farnesyl group intrinsically contains four sets of carbon atoms in a very similar magnetic environment (①CF4 and CF8, ②CF5 and CF9, ③CF6 and CF10, and ④$CF3^1$, $CF7^1$, $CF11^1$, and CF12), it gives rise to a small number of heavily overlapped peaks in the diffusion spectra. Efficient proton-driven spin diffusion of the ^{13}C dipoles through the farnesyl protons also makes the assignments of the ^{13}C signals very difficult. Even under such circumstances, we could identify a pair of intermolecular correlation peaks in the spin-diffusion spectra that were recorded with a mixing time of 100 ms as shown by dashed circles in Figure 2. Along the horizontal line of CF4 and CF8 (see also Figure 1b), we see a correlation peak with $C17^3$ (in the lower field) and the other correlation peak with CF1 (in the higher field). Their intensity decreased to $\sim^1/_4$ upon dilution of [^{13}C]BChl from 100 to 50% (Figure 2). The former peak is missing, but the latter peak stays in the spectra with mixing times of 50 and 250 ms (see panels a and b of Figure 3).

Since we identified such a pair of correlation peaks, we examined if we could find any inter-side chain carbon−carbon short contacts in the set of models used in determining the assembly of the macrocycles. As shown in Scheme 1, the entire side chain attached to the C17 position of the macrocycle consists of the $C17^1-C17^2-C17^3$ acid group and the farnesyl ester group. With regard to the conformation of the side chain closest to the macrocycle (the root region), we assumed the gauche conformations around the $C17-C17^1$

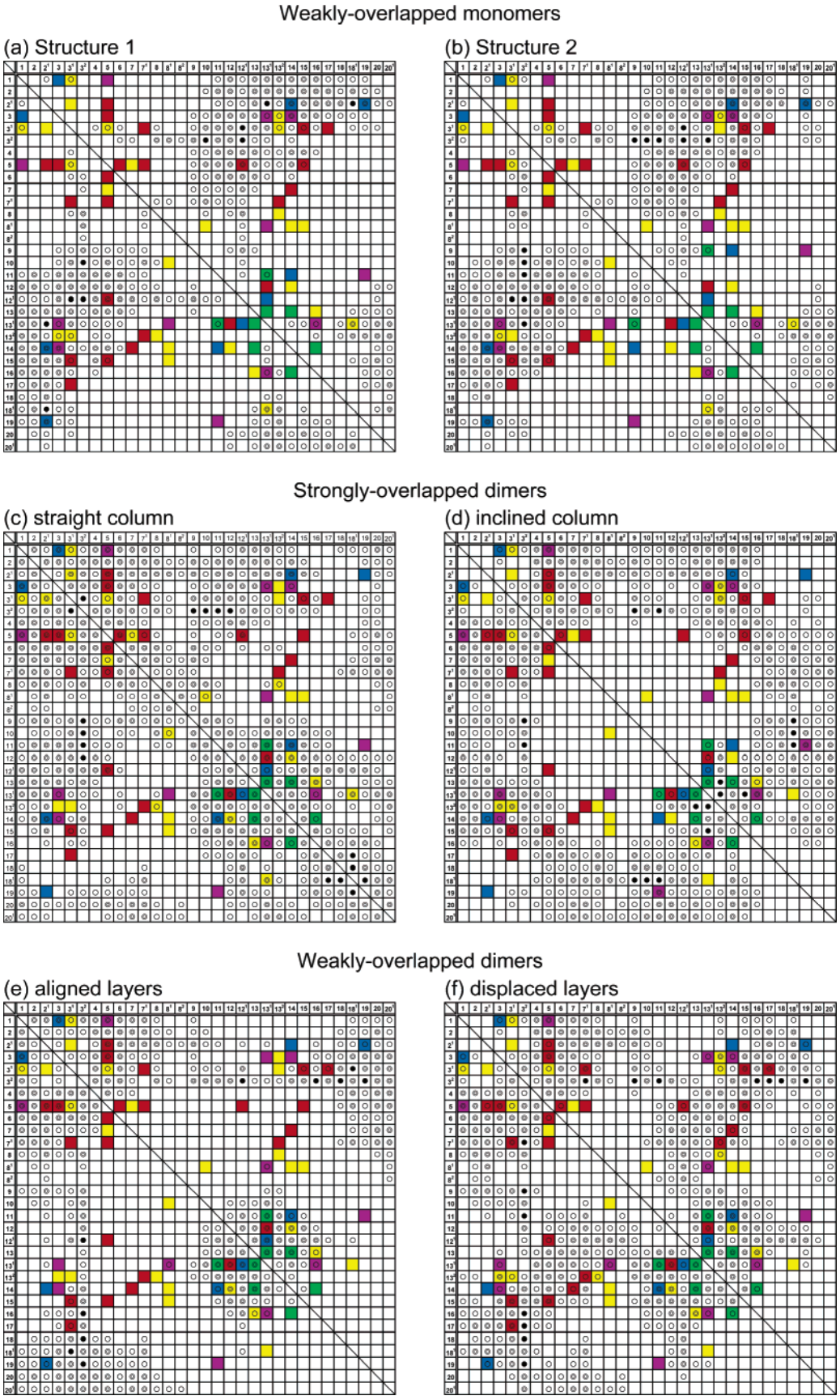

FIGURE 5: Comparison between the observed intermolecular $^{13}C-^{13}C$ correlation peaks and the simulated intermolecular carbon−carbon short contacts, with regard to the macrocycles, based on the models schematically shown in Figure 4. The observed correlation peaks are classified in terms of mixing times when the spin-diffusion spectra are recorded: 50 (yellow), 100 (blue), 250 (red), 50 and 100 (green), and 100 and 250 ms (magenta). The simulated carbon−carbon short contacts are classified by distances: <4 (filled circle), 4−5 (empty double circle), and 5−6 Å (empty circle). The scores of agreement are listed in Table 2.

Table 2: Scores of Agreement for the Prediction of Intermolecular Correlation Peaks for Different Models[a]

	weakly overlapped monomers		strongly overlapped dimers		weakly overlapped dimers	
	structure **1**	structure **2**	straight column	inclined column	aligned layers	displaced layers
50 ms	35%	29%	76%	53%	41%	65%
100 ms	40%	40%	80%	80%	60%	87%
250 ms	32%	32%	68%	64%	55%	91%
average	36%	34%	75%	66%	52%	81%

[a] The scores are defined as the number of correctly predicted peaks divided by the number of total observed correlation peaks.

and $C17^1-C17^2$ rotational axes and the trans conformation for the rest of the side chain, in building the set of models. Although Figure 4 shows only the root of the entire side chain, the trans-zigzag farnesyl group actually stretches downward forming an angle of ~60° with respect to the *Y*-axis in each molecule. Now, we are going to examine the carbon−carbon short contacts between the side chains with regard to the enclosed part of each model in the figure and to correlate them with the observed $^{13}C-^{13}C$ correlation peaks. Figure 6 shows the results (see also Figure 4). (a) In weakly overlapped monomers forming structure **1**, the side chains of the set of three BChl *c* molecules give rise to reasonably short contacts. (b) In weakly overlapped monomers forming structure **2**, on the other hand, the side chains of the set of three BChl *c* molecules give rise to no contacts at all. (c) In strongly overlapped dimers forming a straight column, a pair of BChl *c* molecules is completely overlapped with each other, giving rise to heavily overlapped side chains. This type of molecular assembly can never take place due to severe steric hindrance, as long as we assume the same side chain conformation throughout the aggregate satisfying translational symmetry. (d) Strongly overlapped dimers forming an inclined column as well as (e) weakly overlapped dimers forming aligned layers give rise to interaction between the side chains of the same column of BChl *c* molecules. As a result, the side chains are only in loose contact in both models. (f) In weakly overlapped dimers forming displaced layers, the side chains give rise to three different types of interactions (see Figure 4). (i) The side chains of the four molecules in the dimer-based stacking give rise to contacts such as (e) weakly overlapped dimers forming aligned layers. (ii) The shadowed and (iii) the open monomeric stackings roughly correspond to weakly overlapped monomers in (a) structure **1** and (b) structure **2**, respectively; therefore, they give rise to reasonably short contacts and no contacts at all, respectively. Thus, model f gives rise to a sum of a, b, and e interactions of side chains shown in Figure 6. Thus, weakly overlapped dimers forming displaced layers nicely explain the observed $^{13}C-^{13}C$ dipolar correlations with regard to the side chains; they can be assigned to the $C17^3 \leftrightarrow$ CF4 and CF1 ↔ CF8 correlations. Additional close contacts of the side chains must further stabilize the entire aggregate structure, through van der Waals interaction, as shown in the correlation diagram of Figure 6f.

In conclusion, weakly overlapped dimers forming displaced layers explain the observed intermolecular correlation peaks not only due to the assembly of the macrocycles but also due to the association of the side chains.

Figure 7 shows the structural characteristics of the solid-state aggregate of BChl *c* determined in this investigation (see Figure S1 of the Supporting Information for the entire structure). With regard to the assembly of the macrocycles, this structure includes (i) weakly overlapped dimers that form a column and weakly overlapped monomers somewhat similar to (ii) structure **1** and (iii) structure **2**. With regard to the association of the side chains, close carbon−carbon contacts, i.e., $C17^3 \leftrightarrow$ CF4 and CF1 ↔ CF8 (both 5.5 Å), have been identified by the $^{13}C-^{13}C$ dipolar correlation peaks (see the arrows connecting the pair of carbon atoms in the center bottom panel).[2]

DISCUSSION

Monomer-Based Stacking or Dimer-Based Stacking? The first question we addressed in the introductory section was this long-standing question concerning the structures of in vitro BChl *c* aggregates and chlorosomes. Now, we have obtained a clear answer to this question in the case of the solid-state aggregate consisting of a stereoisomeric mixture of BChl *c* from *Chl. limicola*. The structure has turned out to be a dimer-based stacking of the macrocycles, in which two kinds of monomeric stackings are implicitly incorporated as mentioned above. In building this model, we first assembled piggyback dimers having a pair of Mg···O coordination bonds to form a column and then adjusted the relative positions of the neighboring columns (along the *X*-axis in Figure 4). As a result, a pair of stackings of the macrocycles similar to the monomer-based stackings of structure **1** and structure **2** emerged. However, one has to be aware of the fact that there is little chance of forming real coordination bonds in such shifted assemblies of the macrocycles [see the top views (ii and iii) shown in the bottom part of Figure 7]. Strictly speaking, we should call the assemblies pseudo-monomer-based stackings.

In relation to the dimer-based stacking, we actually observed the splittings of ^{13}C signals in all the PDSD, RFDR, and SPC-5 spectra, which can be explained in terms of the structure described above. It is to be noted that each BChl *c* molecule in the piggyback dimer, as the repeating subunit forming the overall aggregate structure, is symmetrically independent and located in the different magnetic environment. Therefore, the splitting of the $^{13}C-^{13}C$ correlation peaks can be regarded as additional evidence of dimer-based stacking. As schematically shown in Figure 4f, the shaded BChl *c* molecule in the upper part of the dimer, at the bottom, is under the influence of its empty counterpart BChl *c* molecule of the dimer and the neighboring shaded BChl *c* molecules in the structure **1**-type stacking (labeled ii). On the other hand, the empty BChl *c* molecule (on the other side of the dimer) is under the influence of its shaded counterpart and the neighboring empty BChl *c* molecules in the structure **2**-type stacking (labeled iii).

The ring current of the macrocycles can give rise to a very different magnetic environment, and the ring-current effect

[2] A flowchart of model selection and the choice of assignments in overlapped $^{13}C-^{13}C$ correlation peaks according to the model are presented in the Supporting Information to facilitate the readers' critical evaluation of what has been described in Results. We appreciate one of the reviewers for raising questions concerning these points.

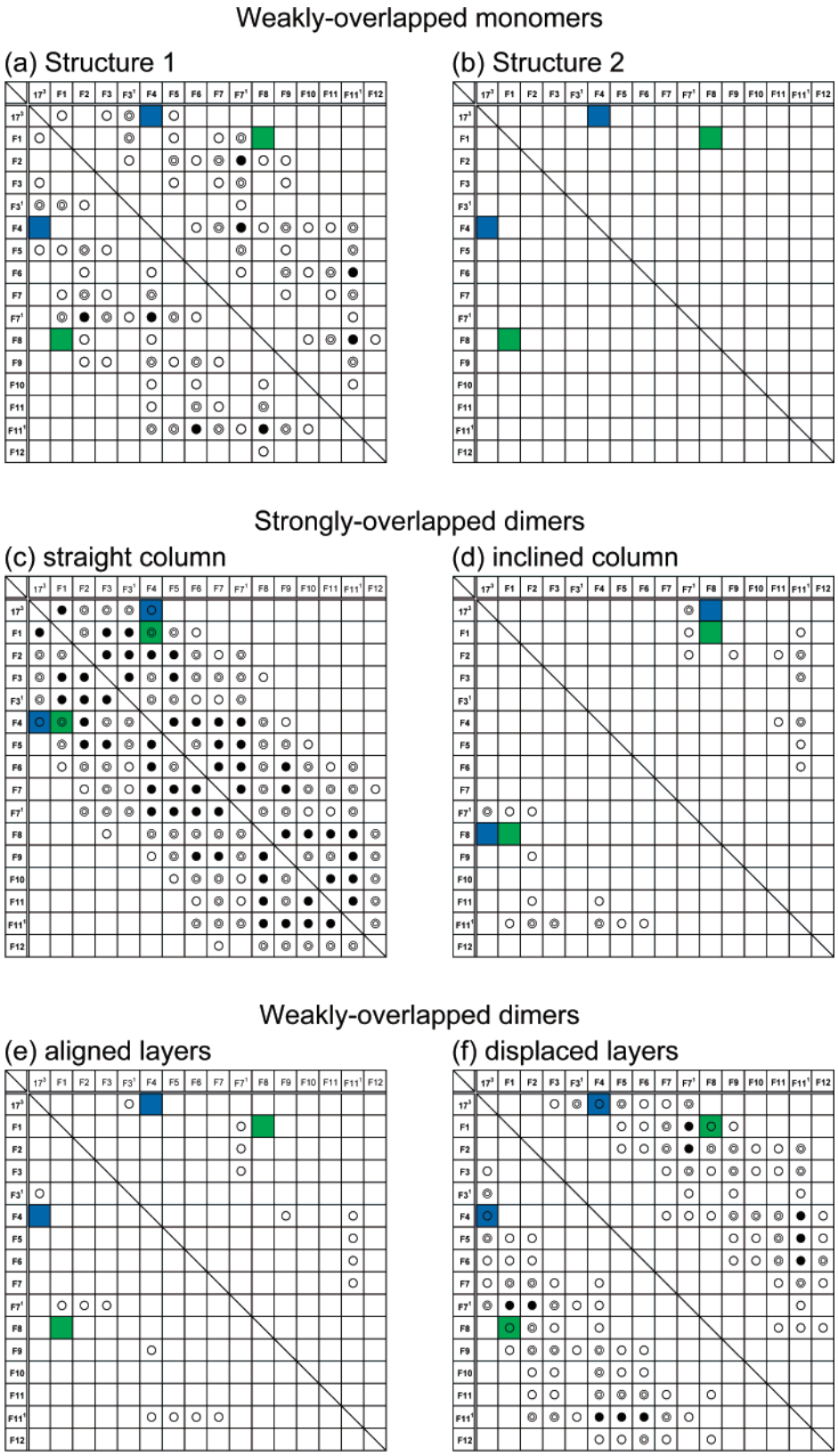

FIGURE 6: Comparison between the observed intermolecular $^{13}C-^{13}C$ correlation peaks and the simulated intermolecular carbon−carbon short contacts, with regard to the side chains, based on the models shown in Figure 4. The observed correlation peaks are classified in terms of mixing times, whereas the simulated carbon−carbon short contacts are classified by distances. See the legend of Figure 5.

on a specified BChl *c* molecule is regarded as a sum of the ring-current effects of all the neighboring BChl *c* molecules in the aggregate. Therefore, as mentioned above, the ring-current effect in each BChl *c* molecule in the dimer is a sum of two different origins, one from the neighboring molecules in the dimer-based stacking and the other from those in the monomer-based stacking of either the structure **1** type or the structure **2** type. Since structure **1** and structure **2** are completely different from each other, the ring-current effect of the dimer-based stacking may become predominant in one

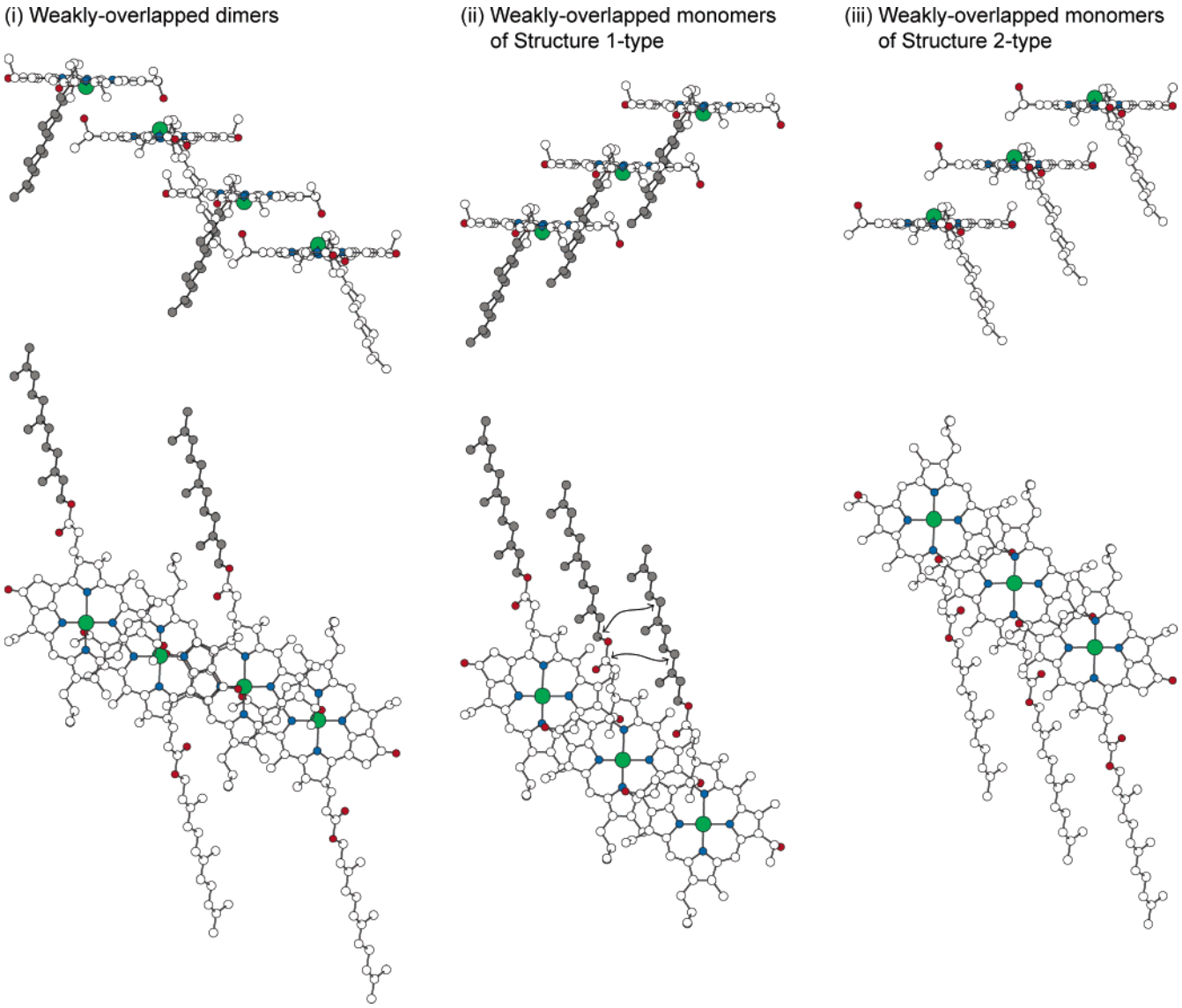

FIGURE 7: Structure of the solid-state aggregate of BChl *c* determined in this investigation (see Figure 4f for its schematic presentation and Figure S1 of the Supporting Information for the details). This structure consists of weakly overlapped dimers forming displaced layers, which includes (i) the stacking of weakly overlapped dimers as well as the stackings of weakly overlapped monomers of (ii) the structure **1** type and (iii) the structure **2** type. The contacts between a pair of side chains giving rise to the observed $^{13}C-^{13}C$ correlation peaks, in panel ii, are shown by a pair of arrows (see the center bottom panel).

BChl *c* molecule, whereas the ring-current effect of the pseudo-monomer-based stacking may become predominant in the other BChl *c* molecule.

It is interesting, in this relation, that Umetsu et al. (*20*) have identified two different types of signals named "type A" and "type B" in the aggregate of *R*[E,E]. Although the authors ascribed the sets of signals to the dimer-based and monomer-based stackings in different solid-state species in the aggregate of BChl *c*, these considerations concerning the NMR spectra of the present solid-state aggregate of BChl *c* show that the sets of signals can be explained in terms of a single, homogeneous aggregate structure. If the sets of signals were originating from the two different solid-state species, the NMR signals should consist of three sets of signals (one for the monomer-based stacking and two for the dimer-based stacking) or two sets of signals with completely different intensities (due to the overlap of the monomeric component with the one of the dimeric components). The authors actually found multiple splitting of the signals, which could be approximated by two major components. This issue needs to be examined further.

As the answer to the first question addressed in the introductory section, it is concluded that the solid-state aggregate of BChl *c* consists of dimer-based stacking to form a column, but it also contains two different types of pseudo-monomer-based stackings with the molecules in the neighboring columns.

Intermolecular Interactions Stabilizing the Solid-State Aggregate of BChl c. The second question we addressed in the introductory section was concerned with the comparison of the structure of the large aggregate in the solid state to that of smaller aggregates in suspension and the examination of intermolecular interactions stabilizing the two structures. Those intermolecular interactions specifically stabilizing the former can be called "the size effects"; they should be inherent to the repeating subunit forming translational symmetry and additive when a seed structure grows to form a larger aggregate. (1) The first is van der Waals (dispersive)

interaction among the π-conjugated macrocycles. When we disregard the orientation of the BChl *c* molecule, the weakly overlapped monomers and the weakly overlapped dimers can be considered to be essentially the same stairlike stacking of the macrocycles (vide supra). This type of stacking probably achieves the best electrostatic stabilization of the π-conjugated macrocycles, because those aggregates give rise to the largest red shift of the Q_y absorption to ~745 nm. (2) The second is a pair of coordination bonds to stabilize the piggyback dimers. The piggyback dimer is the most stable structural motif when the *R*-isomers are predominant (*13*−*16*). (3) The third is assembly of piggyback dimers forming the displaced layers. In this solid-state aggregate of BChl *c*, the pair of coordination bonds alternately connects every pair of layers piling up to the *Z*-direction (Figure 4f). No interdimer cracking along the horizontal planes should easily take place in contrast to the case of weakly overlapped dimers forming aligned layers, for example. Therefore, such a shift of the neighboring columns, by one BChl *c* molecule, must substantially stabilize the overall structure. (4) The fourth is van der Waals interaction between the pairs of neighboring side chains. As shown in Figure 7, a pair of side chains attached to the macrocycles, forming weakly overlapped monomers of the structure **1** type, are associated with each other through van der Waals interaction. The close contacts of the C17[3]···CF4 and CF1···CF8 pairs, identified as the $^{13}C-^{13}C$ dipolar correlation in the spin-diffusion spectra (vide supra), can stabilize the particular stacking of the macrocycles. Other carbon−carbon contacts between the parallel side chains (Figure 6f) may further stabilize the overall aggregate structure.

Among all those intermolecular interactions, (1) the pair of Mg···O coordination bonds to form a piggyback dimer and (2) van der Waals interaction among the π-conjugated macrocycles must stabilize even smaller aggregates in suspension, whereas (3) the assembly of dimers to form displaced layers and (4) van der Waals interaction between the pairs of side chains may additionally stabilize the two-dimensional assembly of the solid-state aggregate of BChl *c*. The latter two intermolecular interactions may be classified as the size effects. (After building the model of the solid-state aggregate of BChl *c*, we identified a pocket that accommodates a water molecule between the pair of hydroxyethyl OH groups, which may form a hydrogen-bonding bridge.)

CONCLUSION

The assembly of an isomeric mixture of BChl *c* extracted from *Chl. limicola* in the solid state has been examined by MAS ^{13}C NMR spectroscopy using the PDSD technique. The intermolecular $^{13}C-^{13}C$ dipolar correlation peaks extracted from the spin-diffusion spectra by the dilution method were compared with the simulated intermolecular carbon−carbon short contacts for a set of models. The analysis has led us to a new type of assembly of BChl *c* molecules, which we call weakly overlapped dimers forming displaced layers. It consists of a dimer-based stacking to form an inclined column, and those columns are aligned to form pseudo-monomer-based stackings of the structure **1** type and the structure **2** type. The above-mentioned structural characteristics are shown in Figure 7. (The overall assembly of BChl *c* molecules is schematically depicted in Figure 4f and the detailed structure in Figure S1 of the Supporting Information.)

This technique has proven to be powerful in determining the real structure of chlorosomes as well, when the replacement of [^{12}C]BChl *c* with [^{13}C]BChl *c* has become feasible via the development of a reconstitution technique. As shown in the case of the in vitro aggregate, it is crucial to correctly select the intermolecular $^{13}C-^{13}C$ correlation peaks out of a mixture of intramolecular and intermolecular correlation peaks in the spin-diffusion spectra.

Also, these results have provided us with a unique piece of information relevant to the structure of chlorosomes, because the spectral similarity between chlorosomes and the solid-state aggregate of BChl *c* has been well-documented (*7*−*9*). The structure of the solid-state aggregate of BChl *c* presented here may be used as a starting model in the structural analysis.[3]

SUPPORTING INFORMATION AVAILABLE

Details of spin-diffusion processes reflecting the structure of the BChl *c* aggregate in the solid state (Figures S1−S3), flowchart of model selection and choice of assignments in overlapped $^{13}C-^{13}C$ correlation peaks according to the model (Figure S4), and structural relevance of this BChl *c* aggregate to chlorosomes. This material is available free of charge via the Internet at http://pubs.acs.org.

REFERENCES

1. Blankenship, R. E., Olson, J. M., and Miller, M. (1995) Antenna Complexes from Green Photosynthetic Bacteria, in *Anoxygenic Photosynthetic Bacteria* (Blankenship, R. E., Madigan, M. T., and Bauer, C. E., Eds.) pp 399−435, Kluwer Academic Publishers, Dordrecht, The Netherlands.
2. Olson, J. M. (1998) Chlorophyll organization and function in green photosynthetic bacteria, *Photochem. Photobiol. 67*, 61−75.
3. Blankenship, R. E., and Matsuura, K. (2003) Antenna Complexes from Green Photosynthetic Bacteria, in *Light-Harvesting Antennas in Photosynthesis* (Green, B. R., and Parson, W. W., Eds.) pp 195−217, Kluwer Academic Publishers, Dordrecht, The Netherlands.
4. Nozawa, T., Ohtomo, K., Suzuki, M., Morishita, Y., and Madigan, M. T. (1993) Structures and organization of bacteriochlorophyll *c*'s in chlorosomes from a new thermophilic bacterium *Chlorobium tepidum*, *Bull. Chem. Soc. Jpn. 66*, 231−237.
5. Chiefari, J., Griebenow, K., Griebenow, N., Balaban, T. S., Holzwarth, A. R., and Schaffner, K. (1995) Models for the pigment organization in the chlorosomes of photosynthetic bacteria: Diastereoselective control of *in-vitro* bacteriochlorophyll c_s aggregation, *J. Phys. Chem. 99*, 1357−1365.
6. Mizoguchi, T., Hara, K., Nagae, H., and Koyama, Y. (2000) Structural transformation among the aggregate forms of bacteriochlorophyll *c* as determined by electronic-absorption and NMR spectroscopies: Dependence on the stereoisomeric configuration and on the bulkiness of the 8-C side chain, *Photochem. Photobiol. 71*, 596−609.
7. Nozawa, T., Ohtomo, K., Suzuki, M., Nakagawa, H., Shikama, Y., Konami, H., and Wang, Z.-Y. (1994) Structures of chlorosomes and aggregated BChl *c* in *Chlorobium tepidum* from solid state high resolution CP/MAS ^{13}C NMR, *Photosynth. Res. 41*, 211−223.
8. Balaban, T. S., Holzwarth, A. R., Schaffner, K., Boender, G.-J., and de Groot, H. J. M. (1995) CP-MAS ^{13}C-NMR dipolar correlation spectroscopy of ^{13}C-enriched chlorosomes and isolated bacteriochlorophyll *c* aggregates of *Chlorobium tepidum*: The self-

[3] The structural relevance of this BChl *c* aggregate to chlorosomes is briefly described in the Supporting Information. We appreciate the other reviewer for encouraging us to mention the relevance of this solid-state aggregate of BChl *c* to chlorosomes.

organization of pigments is the main structural feature of chlorosomes, *Biochemistry 34*, 15259−15266.
9. van Rossum, B.-J., Steensgaard, D. B., Mulder, F. M., Boender, G. J., Schaffner, K., Holzwarth, A. R., and de Groot, H. J. M. (2001) A refined model of the chlorosomal antennae of the green bacterium *Chlorobium tepidum* from proton chemical shift constraints obtained with high-field 2-D and 3-D MAS NMR dipolar correlation spectroscopy, *Biochemistry 40*, 1587−1595.
10. Steensgaard, D. B., Wackerbarth, H., Hildebrandt, P., and Holzwarth, A. R. (2000) Diastereoselective control of bacteriochlorophyll *e* aggregation. 3^1-*S*-BChl *e* is essential for the formation of chlorosome-like aggregates, *J. Phys. Chem. B 104*, 10379−10386.
11. Prokhorenko, V. I., Steensgaard, D. B., and Holzwarth, A. R. (2003) Exciton theory for supramolecular chlorosomal aggregates: 1. Aggregate size dependence of the linear spectra, *Biophys. J. 85*, 3173−3186.
12. Holzwarth, A. R., and Schaffner, K. (1994) On the structure of bacteriochlorophyll molecular aggregates in the chlorosomes of green bacteria. A molecular modelling study, *Photosynth. Res. 41*, 225−233.
13. Mizoguchi, T., Limantara, L., Matsuura, K., Shimada, K., and Koyama, Y. (1996) Aggregation forms of 8-ethyl-12-ethyl farnesyl bacteriochlorophyll *c* in methanol-chloroform mixtures as revealed by ^{1}H NMR spectroscopy, *J. Mol. Struct. 379*, 249−265.
14. Wang, Z.-Y., Umetsu, M., Kobayashi, M., and Nozawa, T. (1999) ^{13}C- and ^{15}N-NMR studies on the intact bacteriochlorophyll *c* dimers in solutions, *J. Am. Chem. Soc. 121*, 9363−9369.
15. Wang, Z.-Y., Umetsu, M., Kobayashi, M., and Nozawa, T. (1999) Complete assignment of ^{1}H NMR spectra and structural analysis of intact bacteriochlorophyll *c* dimer in solution, *J. Phys. Chem. B 103*, 3742−3753.
16. Wang, Z.-Y., Kadota, T., Kobayashi, M., Kasuya, A., and Nozawa, T. (2004) NMR relaxation study of the bacteriochlorophyll *c* in solutions, *J. Phys. Chem. B 108*, 15422−15428.
17. Mizoguchi, T., Matsuura, K., Shimada, K., and Koyama, Y. (1996) The structure of the aggregate form of bacteriochlorophyll *c* showing the Q_y absorption above 740 nm: A ^{1}H-NMR study, *Chem. Phys. Lett. 260*, 153−158.
18. Mizoguchi, T., Sakamoto, S., Koyama, Y., Ogura, K., and Inagaki, F. (1998) The structure of the aggregate form of bacteriochlorophyll *c* showing the Q_y absorption above 740 nm as determined by the ring-current effects on ^{1}H and ^{13}C nuclei and by the ^{1}H−^{1}H intermolecular NOE correlations, *Photochem. Photobiol. 67*, 239−248.
19. Mizoguchi, T., Ogura, K., Inagaki, F., and Koyama, Y. (1999) The structure of an aggregate form of bacteriochlorophyll *c* showing the Q_y absorption at 705 nm as determined by the ring-current effects on ^{1}H and ^{13}C nuclei and by ^{1}H−^{1}H intermolecular NOE correlations, *Biospectroscopy 5*, 63−77.
20. Umetsu, M., Hollander, J. G., Matysik, J., Wang, Z.-Y., Adschiri, T., Nozawa, T., and de Groot, H. J. M. (2004) Magic-angle spinning nuclear magnetic resonance under ultrahigh field reveals two forms of intermolecular interaction within CH_2Cl_2-treated (3^1R)-type bacteriochlorophyll *c* solid aggregate, *J. Phys. Chem. B 108*, 2726−2734.
21. Wahlund, T. M., Woese, C. R., Castenholz, R. W., and Madigan, M. T. (1991) A thermophilic green sulfur bacterium from New Zealand hot springs, *Chlorobium tepidum* sp. nov., *Arch. Microbiol. 156*, 81−90.
22. Kakitani, Y., Rondonuwu, F. S., Mizoguchi, T., Watanabe, Y., and Koyama, Y. (2003) Energy dissipations in chlorosomes: Emission from the Q_y state following singlet−singlet and triplet−triplet annihilation reactions in the cylindrical aggregate and its reversible dissociation into the piggy-back dimers, *J. Phys. Chem. B 107*, 14545−14555.
23. Bennett, A. E., Rienstra, C. M., Griffiths, J. M., Zhen, W., Lansbury, P. T., Jr., and Griffin, R. G. (1998) Homonuclear radio frequency-driven recoupling in rotating solids, *J. Chem. Phys. 108*, 9463−9479.
24. Fujiwara, T., Khandelwal, P., and Akutsu, H. (2000) Compound radiofrequency-driven recoupling pulse sequences for efficient magnetization transfer by homonuclear dipolar interaction under magic-angle spinning conditions, *J. Magn. Reson. 145*, 73−83.
25. Hohwy, M., Rienstra, C. M., Jaroniec, C. P., and Griffin, R. G. (1999) Fivefold symmetric homonuclear dipolar recoupling in rotating solids: Application to double quantum spectroscopy, *J. Chem. Phys. 110*, 7983−7992.
26. Szeverenyi, N. M., Sullivan, M. J., and Maciel, G. E. (1982) Observation of spin exchange by two-dimensional Fourier transform ^{13}C cross polarization-magic-angle spinning, *J. Magn. Reson. 47*, 462−475.
27. Henrichs, P. M., Linder, M., and Hewitt, J. M. (1986) Dynamics of the ^{13}C spin-exchange process in solids: A theoretical and experimental study, *J. Chem. Phys. 85*, 7077−7086.
28. Castellani, F., van Rossum, B., Diehl, A., Schubert, M., Rehbein, K., and Oschkinat, H. (2002) Structure of a protein determined by solid-state magic-angle-spinning NMR spectroscopy, *Nature 420*, 98−102.

BI0525728